Inorganic Chemistry

Article

pubs.acs.org/IC

Structural Basis for the Inhibition of Truncated Islet Amyloid Polypeptide Aggregation by Cu(II): Insights into the Bioinorganic Chemistry of Type II Diabetes

Lina Rivillas-Acevedo,*[,†,‡] Carolina Sánchez-López,[†] Carlos Amero,[‡] and Liliana Quintanar*[,†]

[†]Departamento de Química, Centro de Investigación y de Estudios Avanzados (Cinvestav), México, D.F., México

[‡]Centro de Investigaciones Químicas, Instituto de Investigación en Ciencias Básicas y Aplicadas, Universidad Autónoma del Estado de Morelos, Cuernavaca, Morelos México

Supporting Information

ABSTRACT: Type 2 diabetes (T2D) is one of the most common chronic diseases, affecting over 300 million people worldwide. One of the hallmarks of T2D is the presence of amyloid deposits of human islet amyloid polypeptide (IAPP) in the islets of Langerhans of pancreatic β-cells. Recent reports indicate that Cu(II) can inhibit the aggregation of human IAPP, although the mechanism for this inhibitory effect is not clear. In this study, different spectroscopic techniques and model fragments of IAPP were employed to shed light on the structural basis for the interaction of Cu(II) with human IAPP. Our results show that Cu(II) anchors to His18 and the subsequent amide groups toward the C-terminal, forming a complex with an equatorial coordination mode 3N1O at physiological pH. Cu(II) binding to truncated IAPP at the His18 region is the key event for its inhibitory effect in amyloid aggregation. Electron paramagnetic resonance studies indicate that the monomeric Cu(II)-IAPP(15−22) complex differs significantly from Cu(II) bound to mature IAPP(15−22) fibers, suggesting that copper binding to monomeric IAPP(15−22) competes with the conformation changes needed to form β-sheet structures, thus delaying fibril formation. A general mechanism is proposed for the inhibitory effect of copper and other imidazole-binding metal ions in IAPP amyloid formation, providing further insights into the bioinorganic chemistry of T2D.

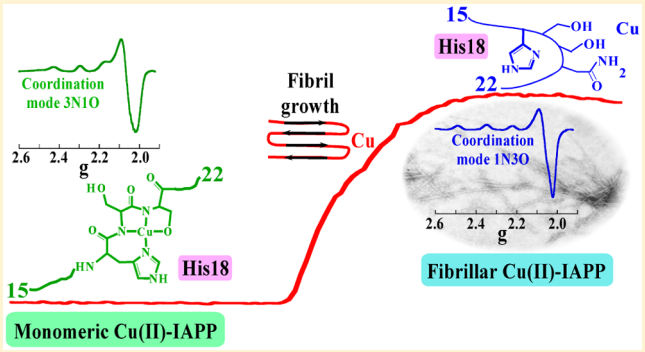

INTRODUCTION

Type 2 diabetes (T2D) is one of the most common chronic diseases. It is a degenerative metabolic disease characterized by elevated blood glucose levels, abnormal insulin secretion, and insulin resistance.[1] One of the hallmarks of T2D is the presence of amyloid deposits of islet amyloid polypeptide (IAPP) in the islets of Langerhans of pancreatic β-cells.[2,3] IAPP, also known as amylin, is a putative polypeptide hormone expressed mainly by the β-cells in humans, and it is stored with insulin in secretory granules.[4,5] The release of IAPP from β-cells occurs in response to nutrient stimuli, as well as insulin.[6] The ratio of IAPP/insulin concentrations is 1:10,[7] while the clearance rates are slower for IAPP.[8] However, the levels of amylin are elevated in conditions associated with insulin resistance, such as obesity[9] and pregnancy.[10] The physiological role of IAPP is not well-understood, but it has been proposed that the peptide is related to glucose metabolism[11] and that it participates in the regulation of food intake, body weight,[12] and renal filtration.[13] Although the physiological activity of amylin is still unknown, clearly the peptide plays a fundamental role in the pathogenesis of T2D, since ∼90% of patients with T2D at autopsy have amyloid deposits, and its degree correlates with the severity of the disease.[14,15]

IAPP sequence is highly conserved among mammalians; however, only IAPP from humans, primates, and cats are able to form amyloid fibrils, whereas IAPP from rodents is not amyloidogenic.[16,17] It is known that the region 20−29 is aggressively amyloidogenic, while fragments 30−37 and 8−20 are also prone to form amyloid fibers.[18] The sequence differences between human and mouse IAPP are the substitution of His18 by Arg in mouse and the presence of three Pro residues within the region of 20−29.[17] The substitution of His18 by Arg does not influence the amyloidogenicity of the fragment 8−20;[18] however, the presence of Pro residues in the 20−29 region preclude the β-sheet conformation necessary for amyloid fibril formation, and it may be the cause of the lack of amyloidogenicity of rodent IAPP.[17]

The IAPP structure in solution is hard to establish by its aggressive propensity to aggregate, even at low concentrations.

Received: December 14, 2014
Published: March 31, 2015

DOI: 10.1021/ic502945k
Inorg. Chem. 2015, 54, 3788−3796

However, NMR experiments have shown that hIAPP on sodium dodecyl sulfate micelles has an overall kinked helix motif.[19] Moreover, some circular dichroism (CD) studies have reported that IAPP is natively disordered in solution,[18,20] although absorption spectroscopy, two-dimensional (2D) infrared spectroscopy and NMR studies show an increase in the helical content prior to its conversion to the β-sheet and fibril conversion.[20−22] In addition, fibrillization studies in the presence of lipids or in aqueous solutions of hexafluoroisopropanol have proved to accelerate the rate of IAPP fibrillization.[23,24] Crystallographic studies of IAPP fused with maltose have shown that IAPP can adopt an α-helical structure at residues 8−18 and 22−27 and that molecules of IAPP dimerize accelerating the fibril formation.[25]

In this context, the role of metal ions in the aggregation of IAPP has become a matter of investigation given that several metal ions have been linked to amyloid aggregation associated with other degenerative diseases, such as Alzheimer, Parkinson and prion diseases.[26,27] The effect of zinc is particularly interesting since it is present in pancreatic β-cells at millimolar levels (granules) and micromolar concentrations (extracellular space),[27,28] while clinical and epidemiological studies suggest Zn deficiency as a common symptom in T2D. On the other hand, in vitro assays show that Zn(II) significantly inhibits IAPP amyloid fibrillogenesis[27] by binding to His18[29] and/or by inhibiting the formation of a dimer that precedes the formation of amyloid fibrils.[30] Some studies show that copper levels are affected in diabetic patients,[31,32] while others affirm that the levels of copper in serum are significantly higher in diabetic patients as compared to healthy individuals,[32−35] suggesting a link between copper homeostasis and the ethiology of T2D. Also, some studies indicate that copper levels affect glycemic control in T2D.[34]

Amyloid-induced toxicity to β-cells is thought to be mediated by increased cellular free radical production,[36] while a role for Cu(II) in the production of reactive oxygen species (ROS) and IAPP amyloid aggregation has been proposed.[35,37,38] However, a recent study revealed that Cu(II) and Ni(II) inhibit IAPP fibrillization and decrease the viability of INS-1 rat insulinoma cells.[39] Both metal ions have very similar binding characteristics, but Ni(II) is not able to catalyze ROS production; thus, the toxicity of Cu(II) was not ascribed to ROS formation but to the stabilization of toxic intermediate species.[39] Consistently, a recent study shows that the Cu(II)-IAPP complex produces hydrogen peroxide to a lesser extent than free Cu(II) in solution, suggesting a sacrificial protective role for IAPP in conditions of high copper concentration.[40]

A potent inhibitory effect of Cu(II) in human IAPP and proIAPP amyloid aggregation has been reported,[37,40−44] while CD studies show that copper induces a more compact conformation with no β-sheet folding.[45] However, the structural details of Cu(II) binding to IAPP remain unknown, impeding further understanding of the mechanism by which Cu(II) inhibits amyloid aggregation. In this study, we employed different spectroscopic techniques to shed light on the structural basis for the interaction of Cu(II) with different fragments of human IAPP. In particular, the effect of Cu(II) in the fibrillization rate and fiber morphology of the human IAPP fragments 15−29 and 15−22 was examined, while direct Cu(II) binding to IAPP(15−22) was investigated in detail. Our results clearly indicate that Cu(II) anchors to His18 in human IAPP fragments in a pH-dependent manner, involving Ser and Asn residues that follow His18 in the sequence, with an equatorial coordination mode 3N1O at physiological pH. Electron paramagnetic resonance (EPR) studies of Cu(II) bound to IAPP(15−22) mature fibrils indicate that Cu(II) coordinated to the monomers competes with the conformation needed to start the formation of β-sheet structure delaying the fibril formation.

EXPERIMENTAL SECTION

Reagents. All chemicals were reagent grade and used without further purification. 9-Fluorenylmethoxycarbonyl (Fmoc) protected amino acids and resins were obtained from Novabiochem (Merck). Water was purified to a resistivity of 18 MΩ/cm using a Millipore deionizing system.

Peptide Synthesis and Purification. The following peptides were synthesized by solid-phase synthesis and Fmoc strategy, as previously described:[46,47] FLVHSSNNFGAILSS (IAPP(15−29)), FLVHSSNN (IAPP(15−22)), FLVH (IAPP(15−18)), FLVASSNN (IAPP(15−22H18A)), HSSNN (IAPP(18−22). All peptides were acetylated at the amino terminus, and the carboxylic terminal was amidated. Crude peptides were purified to >95% by reversed-phase high-performance liquid chromatography and characterized by electrospray ionization mass spectrometry (ESI-MS), as previously described.[48]

Preparation of Peptide Samples. Lyophilized peptides were dissolved in dimethyl sulfoxide (DMSO) to prepare a 15 mM stable stock. Peptide solutions were prepared in a mixture of 20 mM 2-(*N*-morpholino)ethanesulfonic acid (MES) buffer and 20 mM *N*-ethylmorpholine (NEM) buffer. Final concentration for spectroscopic studies was 0.3 mM. For pH titrations, the pH was varied every 0.25 pH units by adding the necessary volume of NaOH or HCl solutions, and it was followed by CD spectroscopy. Peptide samples for EPR spectroscopy were prepared in the same buffer mixture with 50% glycerol to achieve adequate glassing. The addition of glycerol has no effect in the structure of the Cu(II)-peptide complexes, as evaluated by absorption and CD spectroscopy. Fiber samples for EPR were prepared by spinning down aggregates and resuspending pellets in 200 μL of NEM/MES buffer with 50% glycerol.

Thioflavin T Fluorescence Assay. The kinetics of IAPP(15−22) and IAPP(15−29) fragments amyloid formation were monitored by the Thioflavin T (ThT) assay, as an increase in fluorescence emission at 485 nm occurs when the amyloid-specific dye ThT binds to an amyloid fiber. The assay was performed using a Cary Eclipse fluorimeter, at an excitation wavelength of 440 nm. The peptides were diluted in the previously described mixture of buffers at pH 7.5 to a final concentration of 10 μM IAPP(15−29) or 100 μM IAPP(15−22), 25 μM ThT, and the appropriate amount of $CuCl_2$ to have 0.0, 0.5, 1.0, and 2.0 equiv of Cu(II). Fluorescence emission at 485 nm was monitored over time at 37 °C and constant agitation.

Transmission Electron Microscopy. After the ThT assay, the solutions of IAPP were decanted for a couple of days at 4 °C to obtain the aggregates in a pellet. Then, the pellet was washed with deionized water to remove the ThT as much as possible, and it was decanted for another 2 d at 4 °C. The pellet was gently resuspended in 100 μL of water, and 10 μL of this suspension was loaded onto Formvar-coated copper grids for 1 min, washed twice with 5uL of MQ water, and then negatively stained with 2% uranyl acetate for 1 min. Samples were imaged with a JEOL 1400 EX transmission electron microscope.

Electronic Absorption and Circular Dichroism Spectroscopy. Room-temperature absorption and CD spectra in the UV−visible region were recorded using an Agilent 8453 diode array spectrometer and a Jasco J-815 CD spectropolarimeter, respectively, using 1 cm path length quartz cells.

Electron Paramagnetic Resonance Spectroscopy. X-band (9.4 GHz) EPR spectra were collected using an EMX Plus Bruker System, with an ER 041 XG microwave bridge and an ER 4102ST cavity. EPR spectra were recorded at 150 K using an ER4131VT variable-temperature nitrogen system. The samples were run using microwave power, 10 mW; modulation amplitude, 5 G; modulation frequency, 100 kHz; time constant, 327 ms; conversion time, 82 ms; and averaging over 6−12 scans.

DOI: 10.1021/ic502945k
Inorg. Chem. 2015, 54, 3788−3796

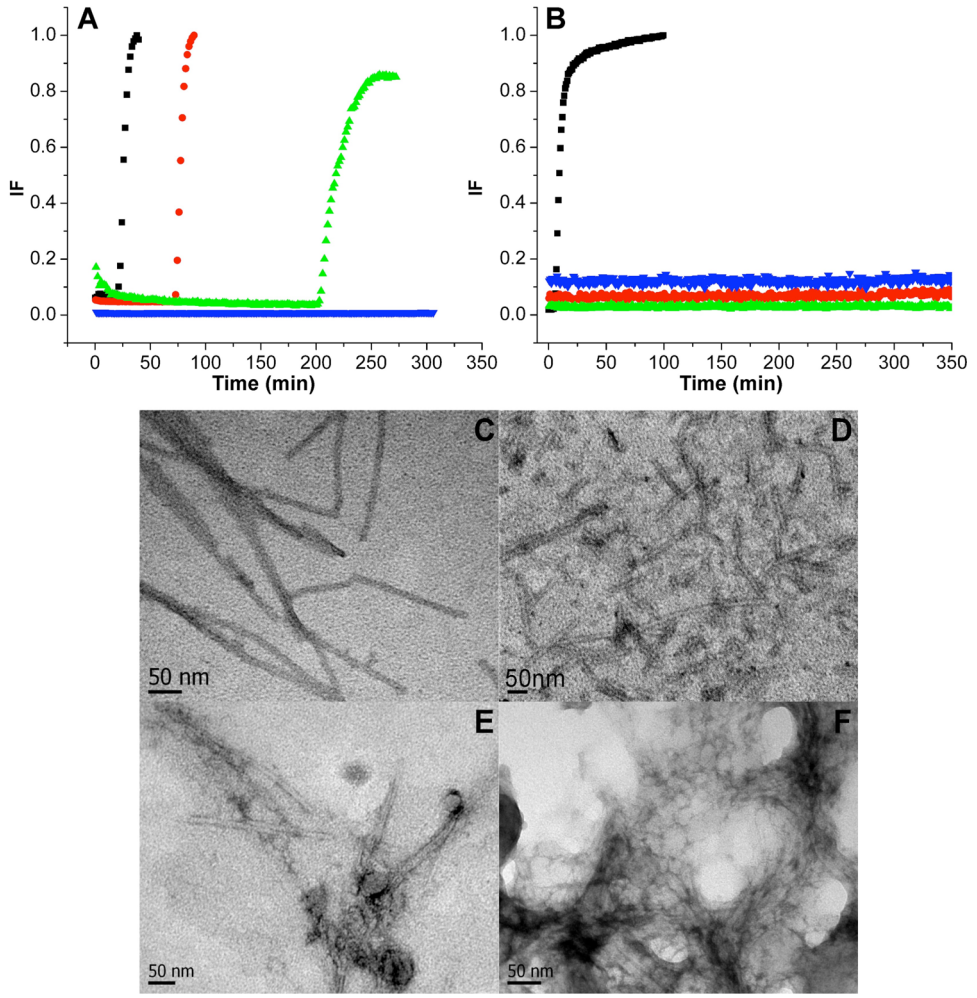

Figure 1. Cu(II) effects in the amyloid aggregation of IAPP(15−22) (A) and IAPP(15−29) (B), followed by ThT fluorescence, in the absence of Cu(II) (black), and presence of 0.5 equiv (red), 1.0 equiv (green), and 2.0 equiv (blue) of Cu(II). TEM images of the IAPP(15−22) amyloid fibrils grown in the absence of Cu(II) (C), and in the presence of 0.5 equiv (D), 1.0 equiv (E), and 2.0 equiv (F) of Cu(II).

Nuclear Magnetic Resonance Spectroscopy. All NMR spectra were recorded at 25 °C on a Varian 700 MHz VNMR-S spectrometer equipped with a cryogenically cooled triple resonance pulse field gradient probe. 2D ^{1}H−^{1}H total correlation spectroscopy (TOCSY) data were collected on a 0.5 mM solution of IAPP(15−22) in MES at pH 7.5 and 15% D_2O, in the absence and presence of 0.3 equiv of Cu(II). Spectra were processed with NMRPipe and analyzed using CARA.

RESULTS AND DISCUSSION

Cu(II) Effect on IAPP Fibrillization. To characterize the effect of Cu(II) in the amyloid aggregation of human IAPP(15−29) and IAPP(15−22) fragments, the kinetics of fibril formation at pH 7.5 were measured in the presence of 0.0, 0.5, 1.0, and 2.0 equiv of Cu(II), as monitored by ThT fluorescence assay. The concentrations of peptides used were 10 and 100 μM, for IAPP(15−29) and IAPP(15−22), respectively. In these assays, an increase in ThT fluorescence intensity at emission λ = 485 nm is indicative of the formation of rigid amyloid-like structures capable of ThT binding. Figure 1A shows that the fibrillization of IAPP(15−22) is slower in the presence of Cu(II). The lag time for aggregation of IAPP(15−22) is 25 min, and it increases to 129 and 274 min in the presence of 0.5 and 1.0 equiv of Cu(II), respectively. Finally, no changes in the ThT fluorescence are observed in the presence of 2.0 equiv of Cu(II) (Figure 1A) in the time frame of these experiments. These results indicate that Cu(II) delays and/or inhibits the formation of amyloid fibers of IAPP(15−22). The effect of Cu is even more pronounced for the longer fragment IAPP(15−29), as shown in Figure 1B. IAPP(15−29) has a shorter lag time for fibrillization (8.9 min) than IAPP(15−22), even at a 10× lower peptide concentration, which is consistent with having a longer sequence that includes hydrophobic residues. In the presence of Cu(II), IAPP(15−29) does not show any increase in ThT fluorescence, indicating that, under the conditions of this experiment, the peptide does not form amyloid fibrils in the presence of Cu(II) (Figure 1B).

The fibers of IAPP(15−22) were imaged by TEM at the end point of the ThT assay. Figure 1C shows that the IAPP(15−22) fibers are long and well-structured; in the presence of 0.5 equiv of Cu(II) the amount of fibers decreases, and the fibers look shorter (Figure 1D). When the fibers are grown with 1.0 equiv of Cu(II), they are shorter and apparently thinner than the fibers grown without Cu(II), while less-structured non-fibrillar aggregates are observed (Figure 1E). In the presence of 2.0 equiv of Cu(II) the TEM image shows mostly disordered aggregates and very few short and thin fibrils (Figure 1F). Altogether, these results show that Cu(II) delays the formation of amyloid fibrils of IAPP, possibly by promoting a different

DOI: 10.1021/ic502945k
Inorg. Chem. 2015, 54, 3788−3796

aggregation pathway that yields fewer and shorter fibrils, as well as aggregates with nonfibrillar morphology.

Cu(II) Binding to IAPP(15−22). To gain insight into the mechanism by which Cu(II) affects the aggregation of IAPP, the direct interaction of this metal ion with IAPP(15−22) was investigated. CD spectroscopy is a useful tool to probe copper-protein interactions, as it allows the characterization of electronic transitions associated with the resulting chiral complexes. Here, a 0.3 mM solution of IAPP(15−22) was titrated with Cu(II) at pH 7.5, followed by electronic absorption and CD spectroscopy (Figure 2). Upon addition

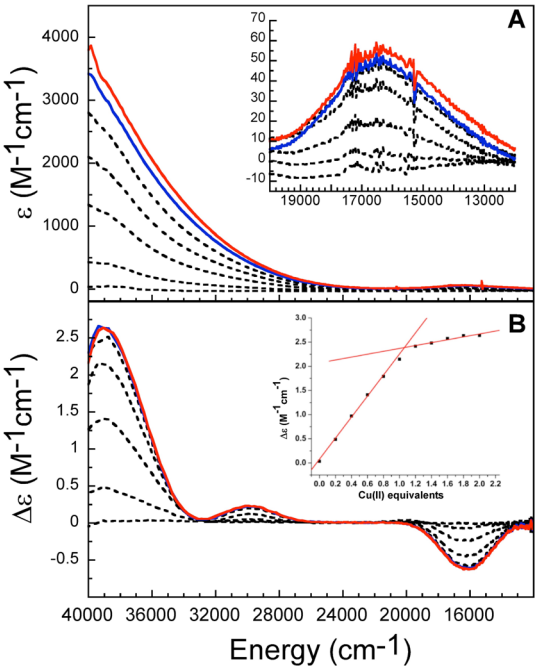

Figure 2. Titration of IAPP(15−22) with Cu(II) followed by UV−vis absorption (A) and CD spectroscopy (B) at pH 7.5. Dotted lines correspond to the addition of 0, 0.2, 0.4, 0.6, 0.8 eq of Cu(II), and the solid blue and red lines correspond to the addition of 1.0 and 2.0 eq of Cu(II), respectively. (A, inset) Enlarged lower-energy region for the d−d region of the UV−vis spectrum (A). (B, inset) CD signal intensity at 39 062 cm^{-1} plotted as a function of the number of equivalents of Cu(II), clearly showing a 1:1 stoichiometry for the Cu−peptide complex.

of the metal ion, several signals arise in the UV−visible region, indicating coordination to the peptide. All CD signals saturate at 1 equiv of Cu(II), suggesting a 1:1 molar stoichiometry for the Cu(II)−peptide complex. The presence of a 1:1 Cu−peptide aduct was confirmed by mass spectrometry, while no evidence for dimeric species was found (Supporting Information, Figure S1). The CD spectrum of the Cu(II)-IAPP(15−22) complex (Figure 2 and Supporting Information, Figure S1) has two negative bands centered around 16 200 cm^{-1} (617 nm; $\Delta\varepsilon$ = −0.71 M^{-1} cm^{-1}), and 32 400 cm^{-1} (309 nm; $\Delta\varepsilon$ = −0.024 M^{-1} cm^{-1}); and a couple of positive signals around 29 800 cm^{-1} (335 nm; $\Delta\varepsilon$ = 0.14 M^{-1} cm^{-1}), and at 39 000 cm^{-1} (256 nm, $\Delta\varepsilon$ = 2.64 M^{-1} cm^{-1}) (Supporting Information, Table S1). On the basis of their energies and intensity, the electronic transition at 16 200 cm^{-1} can be assigned as a d−d band, while all others correspond to ligand-to-metal charge transfer (LMCT) transitions. In particular, transitions at 32 400 and 39 000 cm^{-1} can be assigned as π_1 and π_2 LMCT that originate from imidazole His binding to Cu(II),[49] while the signal at 29 800 cm^{-1} is a LMCT indicative of coordination of deprotonated amide groups.[49] Finally, once the CD signals associated with the Cu(II)-IAPP(15−22) complex were identified, their growth as a function of Cu concentration was used to estimate a dissociation constant (K_d) for this complex. Assuming only one binding site, a fit of the titration data yielded a K_d of 12.3 ± 2.7 μM for the Cu(II)-IAPP(15−22) complex (Supporting Information, Figure S2).

Often, Cu(II) coordination to peptides is pH-dependent; therefore, the CD spectrum of the Cu(II)-IAPP(15−22) complex was collected at different pH values (Figure 3).

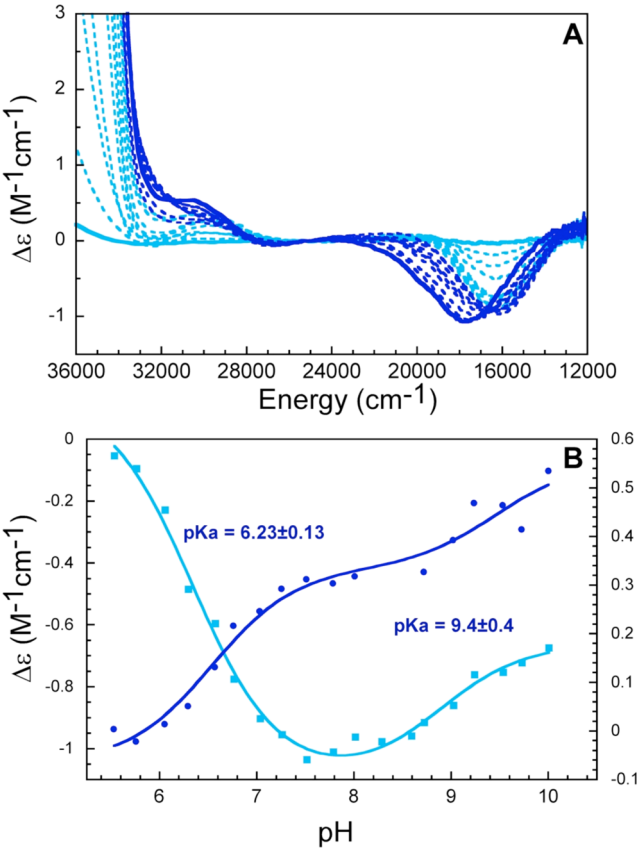

Figure 3. pH titration of the Cu(II)-IAPP(15−22) complex (A), as followed by CD. The Cu(II)-IAPP complex solution was titrated from pH ≈ 5.7 (continuous bold light line) to pH ≈ 10 (continuous bold dark line); spectra for intermediate pH values are shown in dashed lines. The traces for the CD signal intensity changes at 16 234 cm^{-1} (light blue and left Y axis scale) and 30 303 cm^{-1} (dark blue and right *Y*-axis scale) (B) were fitted to the model described in the text (solid lines) to determine the associated pK_a values.

Following the CD spectral changes at different energies, it becomes evident that the signal intensity is dependent on pH, and the signal displays a sigmoidal behavior, which is indicative of protonation equilibria. The experimental data can be fit with the following model:

$$\Delta\varepsilon_{obs} = \frac{(\Delta\varepsilon_1 2[H^+] + \Delta\varepsilon_2[H^+]Ka_1 + \Delta\varepsilon_3 Ka_1 Ka_2)}{(2[H^+] + [H^+]Ka_1 + Ka_1 Ka_2)} \quad (1)$$

where $\Delta\varepsilon_{obs}$ is the observed CD signal intensity at any given pH, Ka_1 and Ka_2 are equilibrium constants associated with two protonation events of the Cu(II)-IAPP complex, and $\Delta\varepsilon_1$, $\Delta\varepsilon_2$,

DOI: 10.1021/ic502945k
Inorg. Chem. 2015, 54, 3788−3796

and $\Delta\varepsilon_3$ are the CD signal intensities of the three different species with different protonation states. The pK_a values associated with the two protonation equilibria, as determined by the best fit of experimental data from at least duplicated experiments, are 6.23 ± 0.13 and 9.42 ± 0.4. These results indicate that at physiological pH (7.4), only one species of the Cu(II)-IAPP(15−22) complex is present.

Cu(II) coordination to IAPP(15−22) at pH 6.0, 6.5, 7.5, 8.5, and 9.5 was also studied by X-band EPR (Figure 4 and

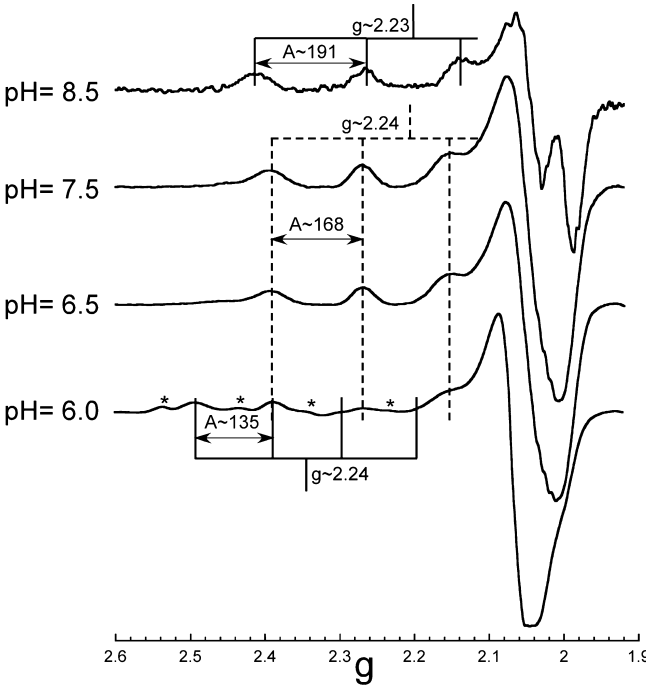

Figure 4. EPR spectra of the Cu(II)-IAPP(15−22) complexes at different pH values. All spectra were collected as described in the experimental section at 150 K. Asterisks indicate signals associated with free Cu(II) in solution.

Supporting Information, Table S2) to get further insight into the protonation equilibriums observed by CD. In all cases, the complexes show EPR signals with $g_{II} > g_{\perp} > 2.00$ and a large parallel copper hyperfine splitting (A_{II}), which is indicative of a $d_{x^2-y^2}$ ground state. At pH 7.5, only one Cu(II)-IAPP(15−22) complex is observed with g_{II} and A_{II} values of 2.236 and 168 × 10^{-4} cm^{-1}, falling in a range associated with complexes with an equatorial coordination mode with three nitrogen-based and one oxygen-based ligands (Table S2), according to Peisach−Blumberg correlations.[50] Note that this type of correlation is only informative of the equatorial coordination shell, and thus, the possibility of the presence of a fifth axial ligand in this complex cannot be evaluated by these correlations.

In contrast, at pH 6.0, three species are observed: (i) signals associated with free Cu(II) in solution; (ii) a species with g_{II} = 2.374 and A_{II} = 135 × 10^{-4} cm^{-1} that correlates to an equatorial coordination shell with one nitrogen and three oxygen-based ligands (1N3O); and (iii) a species with g_{II} = 2.237 and A_{II} = 167 × 10^{-4} cm^{-1} that correlates to an equatorial coordination shell of 3N1O, and it actually corresponds to the species found at pH 7.5 (Figure 4 and Supporting Information, Table S2). The 1N3O complex must be Cu(II) bound to His18, where the oxygen-based ligands could be provided by the solvent or the peptide. Thus, the pK_a of 6.23 can be associated with the concerted deprotonation of two backbone amides to transform the 1N3O complex into the 3N1O complex, which is the actual chiral complex detected by CD. IAPP is stored in β-cell granules at pH ≈ 5.5, and it is released into the extracellular compartment where the pH is 7.4. Thus, the 1N3O and 3N1O complexes are physiologically relevant species.

Finally, EPR data collected at pH 8.5 and 9.5 reveal the presence of another species with g_{II} = 2.223 and A_{II} = 220 × 10^{-4} cm^{-1} that correlates to an equatorial coordination mode with four nitrogen-based ligands (4N), according to Peisach−Blumberg correlations (Figure 4 and Table S2). Thus, the pK_a of 9.2 can be ascribed to the deprotonation of a backbone amide in the 3N1O complex to lead to a 4N complex. However, the 4N species would not be relevant under physiological conditions.

His18 is a Key Residue for Cu(II) Binding to IAPP(15−22) and Its Effect on Aggregation. To evaluate the role of His18 in Cu(II) binding to IAPP(15−22), the IAPP(15−22)H18A variant was prepared. A comparison of the CD spectra of the Cu(II) complexes at pH 7.5 (Figure 5A) shows changes upon the H18A substitution: the transition at 16 200 cm^{-1} is shifted to 17 100 cm^{-1} and is less intense (585 nm $\Delta\varepsilon$ = −0.23 $M^{-1}cm^{-1}$); the band around 29 800 cm^{-1} is shifted to higher energy, while all the transitions show significantly decreased intensity (Supporting Information, Table S1). All these differences indicate that the nature of the Cu(II)-IAPP(15−22) complex has been drastically affected upon the H18A substitution. The EPR spectra show even more dramatic differences (Figure 5B): the g_{II} and A_{II} values for the Cu(II)-IAPP(15−22)H18A complex are 2.221 and 201 × 10^{-4} cm^{-1}, which are widely different from those obtained for the Cu(II)-IAPP(15−22) complex, and fall in a range associated with an equatorial coordination with four nitrogen-based ligands (Supporting Information, Table S2). In fact, these parameters are similar to those obtained in a recent study of rat IAPP, which lacks residue His18.[47] Finally, the decreased intensity of the CD and EPR spectra of the Cu(II)-IAPP(15−22)H18A complex suggests a diminished affinity for Cu(II). Overall, these results indicate that His18 is the primary anchoring residue for Cu(II) binding to IAPP(15−22) and that the absence of His18 leads to the formation of a completely different Cu(II)-IAPP complex.

We next evaluated the effect of Cu(II) ions in the aggregation of IAPP(15−22)H18A (Supporting Information, Figure S3). Addition of Cu(II) delays the formation of IAPP(15−22)H18A amyloid fibers but to a lesser extent as compared to wild type IAPP(15−22). In fact, while addition of 2 equiv of Cu(II) completely abates fibrillization of IAPP(15−22), it does not prevent formation of amyloid fibrils with IAPP(15−22)H18A (Figure S3). A recent spectroscopic study has shown that Cu(II) binds to rat IAPP(17−22) fragment, even in the absence of anchoring groups like His18, potentially coordinating to Ser and Asn residues in positions 19 to 22.[47] Thus, Cu(II) binding to these residues must be responsible for the weak effect of this metal ion in the aggregation of IAPP(15−22)H18A. In summary, our results indicate that the H18A substitution diminishes the affinity of the peptide for Cu(II), leading to a completely different Cu(II)-IAPP complex, and diminishing significantly the inhibitory effect of Cu(II) in IAPP amyloid formation.

Identifying Other Key Residues for Cu(II) Binding to IAPP(15−22). When Cu binds to His-containing peptides, its coordination shell can be completed by deprotonated backbone

DOI: 10.1021/ic502945k
Inorg. Chem. 2015, 54, 3788−3796

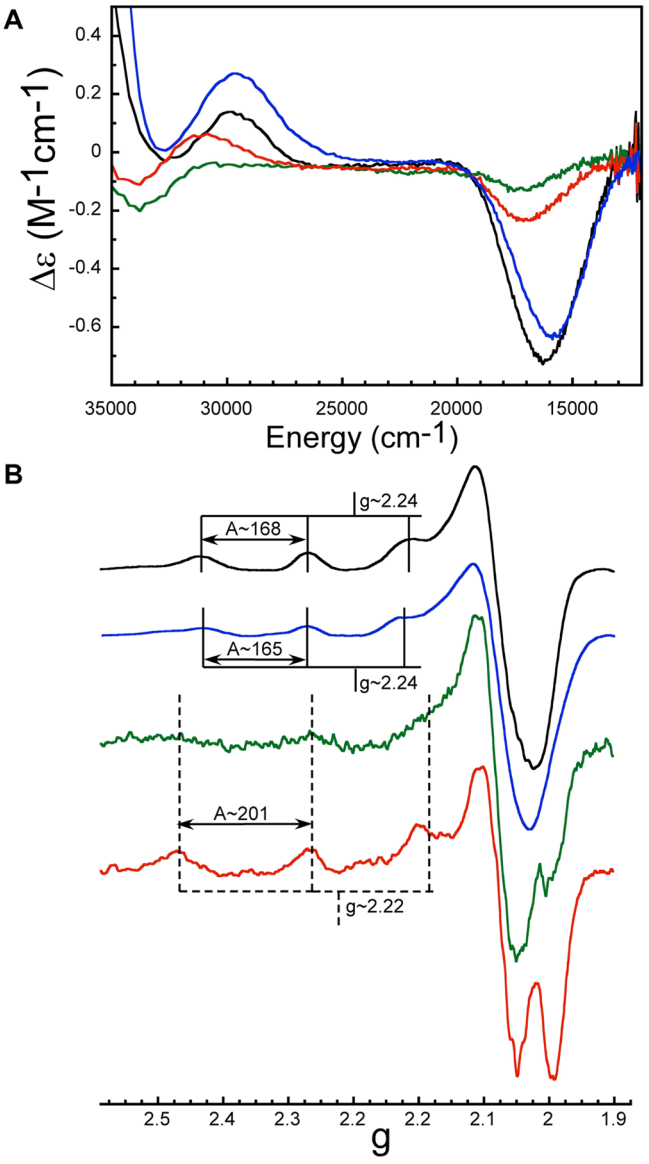

Figure 5. CD (A) and EPR spectra (B) of Cu(II) complexes with human IAPP fragments: 15−22 (black), 18−22 (blue), 15−18 (green), and 15−22H18A (red). All spectra were collected after the addition of 1.0 equiv of Cu(II) at pH 7.5.

amide groups and/or amino acid residues in the vicinity.[46] To evaluate the role of the residues that precede and follow His18 in the sequence in Cu(II) binding to IAPP(15−22), the shorter fragments IAPP(18−22) and IAPP(15−18) were prepared. The CD spectra of the Cu(II) complexes with these variants are compared at pH 7.5 in Figure 5A, clearly showing the similarities between the IAPP(18−22) and IAPP(15−22) Cu(II) complexes (Supporting Information, Table S1). Moreover, the EPR parameters for these two complexes are very similar, and in both cases, their parallel g and A values correlate well for complexes with a 3N1O equatorial coordination mode (Figure 5B and Supporting Information, Table S2). In contrast, the CD spectrum of the Cu(II)-IAPP(15−18) complex (Figure 5B) is strikingly different from that of Cu(II)-IAPP(15−22), showing two negative signals around 17 250 cm^{-1} (580 nm; $\Delta\varepsilon$ = −0.13 M^{-1} cm^{-1}) and 33 900 cm^{-1} (295 nm; $\Delta\varepsilon$ = −0.19 M^{-1} cm^{-1}) (Table S1). Furthermore, EPR indicates the differences between the two complexes are dramatic, as the EPR parameters of the Cu(II)-IAPP(15−18) complex fall in a range associated with a 4N equatorial coordination (Table S2) at pH 7.5.

Overall, these data indicate that the Cu(II) complex formed with IAPP(18−22) has the same coordination environment as the Cu(II)-IAPP(15−22) complex. This conclusion is further supported by an analysis of the titration data of the Cu(II)-IAPP(18−22) complex, which yields a very similar K_d value (7.1 ± 1.5 μM) to that of the Cu(II)-IAPP(15−22) complex (Supporting Information, Figure S2). It becomes evident then, that the residues following His18 are key for Cu(II) binding to IAPP, while residues preceding His18 are not required for Cu(II) coordination. To further test this notion, 2D ^{1}H−^{1}H TOCSY NMR data were collected on the IAPP(15−22) peptide (Figure 6). Signal assignment was adjusted to our

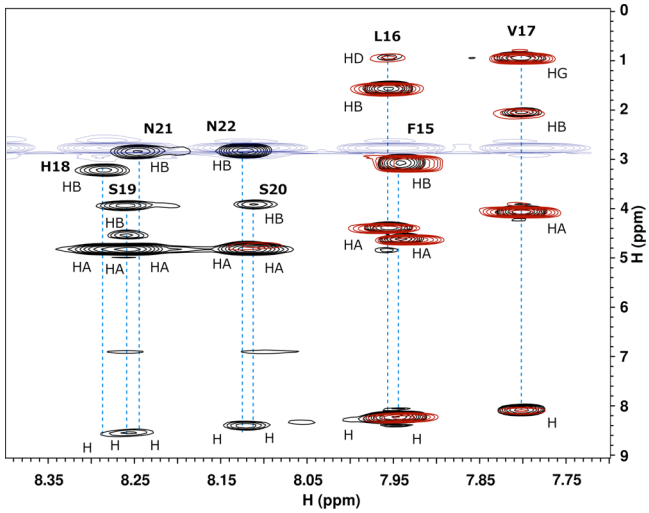

Figure 6. Overlaid 2D ^{1}H−^{1}H TOCSY NMR spectra of IAPP(15−22) in the absence (black) and presence (red) of 0.3 equiv of Cu(II). Signals labeled as H correspond to backbone amide protons for each residue, while HA, HB, HG, and HD correspond to α, β, γ, and δ protons, respectively, the latter being only relevant for Leu and Val residues. Blue signals correspond to noise from residual DMSO in the peptide solution.

conditions from the BMRB-18795 assignment.[51] ^{1}H−^{1}H TOCSY allows the observation of cross peaks for the backbone amide groups of each residue (denoted as H in Figure 6), as well as the protons placed at positions α, β, γ, and δ with respect to the backbone carbonyl group (denoted as HA, HB, HG, and HD, respectively, in Figure 6). Upon addition of 0.3 equiv of Cu(II), the signals from residues His18, Ser19, Ser20, Asn21, and Asn22 disappear completely, while those of residues Phe15, Leu16, and Val17 are not affected at all (Figure 6). Since Cu(II) is a paramagnetic ion, its binding to the peptide would cause a decrease in intensity of the signals of the residues in the vicinity of its binding site; this is due to the paramagnetic relaxation enhancement (PRE) effect.[52] Thus, the data shown in Figure 6 strongly support the conclusion that Cu(II) binding to the IAPP(15−22) occurs toward the C-terminal of the peptide, involving residues His18, Ser19, Ser20, Asn21, and Asn22, while the residues preceding the His18 are not involved in Cu(II) binding at all. Although it might be surprising that Cu(II) coordination to a His-containing peptide would occur toward the C-terminal forming a seven-membered ring with the first deprotonated amide, note that the final complex with a

DOI: 10.1021/ic502945k
Inorg. Chem. 2015, 54, 3788−3796

3N1O equatorial coordination mode would form a set of 7,5,5-membered rings (Supporting Information, Figure S4). Such a chelate would be overall more stable than the set of 6,5,7-membered rings that would be formed for a 3N1O complex toward the N-terminal, considering the participation of two deprotonated amide groups and a backbone carbonyl.[53]

Altogether, our spectroscopic data indicate that (i) Cu(II) binds to His18 and the residues toward the C-terminal domain; (ii) Cu(II) coordination involves deprotonated backbone amide groups; and (iii) the equatorial coordination shell involves three nitrogens and one oxygen-based ligand, at physiological pH. Thus, two plausible coordination models for the Cu(II)-IAPP(15−22) complex at pH 7.5 can be proposed, with Cu(II) binding to His18 and the deprotonated amides of Ser19 and Ser20. To complete the 3N1O equatorial coordination mode, the oxygen-based ligand could be a backbone carbonyl, the hydroxyl group of Ser 20, or a water molecule. The proposed structures are shown in Supporting Information, Figure S4, although further studies are needed to probe the specific role of Ser and Asn residues that follow His18 in the Cu(II) coordination shell.

Cu(II) Bound to IAPP Aggregates. Once a good description for Cu(II) coordination to monomeric IAPP has been achieved, the characterization of how Cu(II) binds to IAPP aggregates should shed light on the mechanism for Cu-mediated inhibition of IAPP amyloid formation. Thus, the EPR spectra of fibers of IAPP(15−22) grown in the presence of 0.5 equiv of Cu(II) at pH 7.5 were collected (Figure 7). The g_{II} and

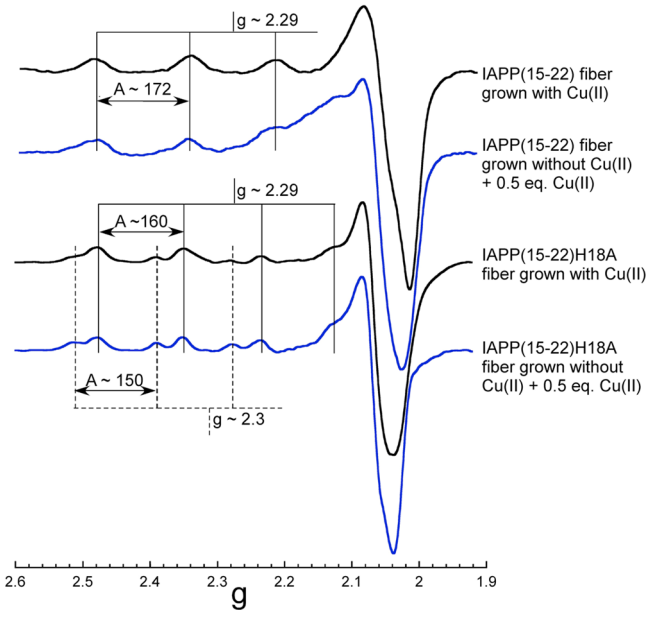

Figure 7. EPR spectra for Cu(II) bound to IAPP(15−22) and IAPP(15−22)H18A fibers at pH 7.5. Spectra in black correspond to fibers grown in the presence of 0.5 equiv of Cu(II), while spectra in blue correspond to fibers grown in the absence of metal ion; however, 0.5 equiv of Cu(II) was added once the mature fiber was formed.

A_{II} of Cu(II) present in the IAPP(15−22) fibers are 2.286 and 172×10^{-4} cm^{-1}; these parameters fall in the range of values associated with 1N3O or 4O equatorial coordination. Clearly, this equatorial coordination is very different from that observed for the Cu(II)-IAPP complex in solution (Table 1). This implies that, even though Cu(II) was initially bound to IAPP(15−22) as characterized for the monomeric peptide in solution, upon aggregation the mode of Cu(II) binding to the peptide changes drastically, leading to a different coordination environment. This would imply that the conformational changes involved in fiber formation forces the metal ion to adopt a coordination mode in the peptide that is very different from the one it would adopt in solution. Consistently, when 0.5 equiv of Cu(II) was added to fibers of IAPP(15−22) grown in the absence of metal ion, the EPR spectrum was dominated by a species with a $g_{II} = 2.285$ and $A_{II} = 172 \times 10^{-4}$ cm^{-1}, which is practically identical to that observed for the fibers grown in the presence of Cu(II) (Figure 7, Table 1), and it is drastically different from the species observed for the monomeric Cu(II)-IAPP(15−22) complex in solution.

Table 1. Electron Paramagnetic Resonance Parameters of Monomeric and Fibrillar Cu(II)-IAPP Complexes at pH 7.5

complex	g_{II}	A_{II}[a]	coordination mode
monomeric Cu(II)-IAPP(15−22)	2.236	168	3NO
IAPP(15−22) fibers grown with Cu(II)	2.286	172	N3O
IAPP(15−22) fibers + Cu added	2.285	172	N3O
	2.319[b]	166[b]	4O[b]
monomeric Cu(II)-IAPP(15−22)H18A	2.221	201	4N
IAPP(15−22)H18A fibers grown with Cu(II)[c]	2.291	160	N3O
	2.336	148	4O
IAPP(15−22)H18A fibers + Cu added[c]	2.292	158	N3O
	2.333	151	4O

[a] ($cm^{-1} \times 10^{-4}$). [b] A very small amount of a second species is observed, which does not correspond to free Cu(II) in solution (Supporting Information, Figure S5). [c] Two different species are observed.

On the other hand, the EPR spectrum of IAPP(15−22)H18A fibers, grown in the presence of Cu(II), shows two species at pH 7.5, one of them with g_{II} and A_{II} values that correspond to a 1N3O equatorial coordination, while the second species corresponds to a 4O equatorial coordination (Figure 7, Table 1). In addition, identical EPR spectra were observed when 0.5 equiv of Cu(II) were added to IAPP(15−22)H18A fibers grown in the absence of metal ions. Evidently, none of these two species correspond to that observed in the Cu(II)-IAPP(15−22)H18A soluble complex at pH 7.5, which displays a 4N equatorial coordination (Supporting Information, Table S2), and they do not correspond to free Cu(II) in solution either (Supporting Information, Figure S5). All these results suggest that Cu(II) coordination to these peptides is different in solution than in the aggregated form. Thus, the fibrillization of IAPP(15−22) has an important impact in metal ion coordination: the Cu(II) binding site in IAPP as characterized in solution is no longer available or accessible to the metal ion in the amyloid fibril. Instead, Cu(II) binds to IAPP fibers yielding coordination modes that are less nitrogen-rich, with 1N3O or 4O equatorial coordination modes.

Mechanism for the Inhibitory Effect of Cu(II) in IAPP Amyloid Aggregation. Our results clearly show that Cu(II) exerts an important effect in the aggregation of IAPP, as manifested by a significant delay in fibrillization and changes in the morphology of the aggregates. A detailed spectroscopic study of Cu(II) binding to IAPP shows that the anchoring residue for this interaction is His18 and that Ser and Asn residues that follow His18 in the sequence (i.e., residues 19−22) also play an important role in Cu binding, while residues preceding His18 are not required for Cu(II) coordination. Cu(II) binding to His18 as characterized in solution is the key

DOI: 10.1021/ic502945k
Inorg. Chem. 2015, 54, 3788−3796

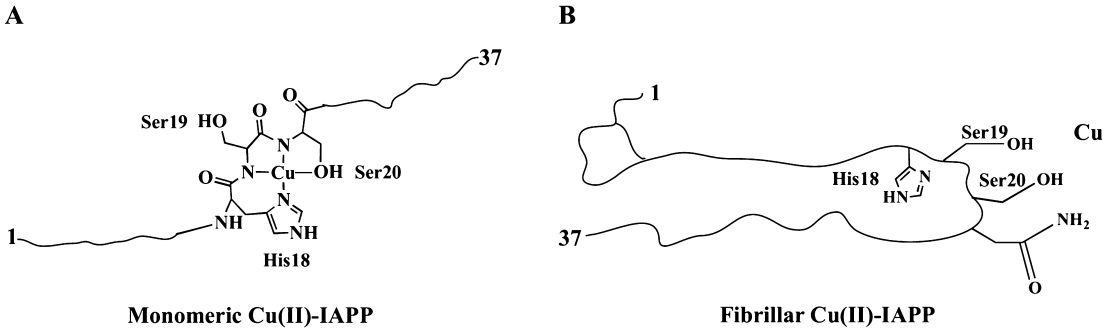

Figure 8. Schematic representation of the conformational change of the peptide bound to Cu(II), from monomeric complex (A) to fibril formation (B). The conformation in (B) is drawn based on the crystal structure of a fibril fragment of IAPP (3FTH).[55]

event that is associated with the effect of this metal ion in IAPP(15−22) fibrillization, as the H18A substitution diminishes the Cu(II) effect. Thus, Cu(II) binds to IAPP(15−22) fragment in a key region for its conversion into amyloid fibers. In fact, fibrillization of IAPP(15−22) forces Cu(II) to adopt a drastically different coordination mode than the original complex in monomeric solution, strongly suggesting that the conformation imposed by copper in the monomeric Cu(II)-IAPP(15−22) complex competes with the conformational changes that are necessary in the aggregation pathway leading to amyloid fibers. Models for IAPP amyloid fibrils have been derived recently by EPR,[54] crystallography,[55] and solid-state NMR.[56] In the latter two models, the His18 residue is located in the inner part of the β-sheet structure, while residues Ser19, Ser20, Asn21, and Asn22 form a loop between two β-sheets. This conformation clearly explains the fibrillization delay caused by copper, since the formation of the β-sheet would compete with the conformation that Cu(II) would impose in the peptide backbone upon binding to His18 and residues 19−22 that follow in the sequence (Figure 8).

From our work it derives that any metal ion anchoring at His18 would have an inhibitory effect in a similar fashion to copper ions. In fact, His18 could be an anchoring residue for Zn(II) and Ni(II) ions, both of them described as inhibitors of IAPP amyloid aggregation. Moreover, a recent study reports the inhibitory effect of a ruthenium complex,[57] which clearly could be binding to His18. Thus, the mechanism described in Figure 8 is certainly a general mechanism for the inhibitory effects of metal ions with imidazole binding properties.

Mature IAPP is stored in the β-cell granules of the pancreas at low pH, and it is normally released into the extracellular compartment, where pH is 7.4.[58] Thus, the spectroscopic characterization of the monomeric Cu(II)-IAPP(15−22) species presented here would be relevant in physiological conditions. Moreover, it is plausible to propose that the inhibitory effect of Cu(II) and Zn(II) ions in IAPP amyloid aggregation via anchoring at His18 could be a mechanism to modulate IAPP conformations and prevent the formation of IAPP fibers. The potential loss of Cu homeostasis in diabetic patients would certainly affect these interactions, particularly when IAPP is released into the extracellular space. On the other hand, it has been proposed that Cu(II)-IAPP complexes could stabilize cytotoxic oligomers that trigger apoptosis[39] or small aggregates that increase IAPP cytotoxicity by generating ROS[38] causing mitochondria disruption,[37] although the molecular details of these processes remain to be investigated. Understanding the physiological relevance of the interaction of Cu(II) with IAPP and how these interactions may play a role in pancreatic degeneration associated with T2D are crucial steps to find therapeutic strategies for this disease.

CONCLUSIONS

Human IAPP is found in the pancreatic islets of patients with T2D as amyloid deposits, and it is thought to play a central role in the disease. Cu(II) inhibits the amyloid aggregation of IAPP, and it induces the formation of small aggregates. Our study shows that Cu(II) binding to IAPP(15−22) at the His18 region is the key event for its inhibitory effect in amyloid aggregation. The residues following His18 are important for Cu(II) binding to IAPP, while residues preceding His18 are not required for Cu(II) coordination. At physiological pH (7.4), Cu(II) anchors to His18 and the subsequent amide groups toward the C-terminal, forming a complex with an equatorial coordination mode 3N1O. Our EPR studies indicate that Cu binding to monomeric IAPP(15−22) in this fashion competes with the conformation changes needed to form β-sheet structures, thus delaying fibril formation. From our work it derives that any metal ion anchoring at His18 would have an inhibitory effect in a similar fashion to copper ions, providing a general mechanism for the inhibitory effects of metal ions with imidazole binding properties. This study sheds light on the structural basis for the interaction of Cu(II) ions with IAPP and their inhibitory effect in its amyloid aggregation providing further insights into the bioinorganic chemistry of T2D.

ASSOCIATED CONTENT

Supporting Information

Electronic transitions for the Cu(II)-IAPP complexes (tabulated data), mass spectrometry analysis of the Cu(II)-IAPP(15−22) complex, estimation of the K_d values for the Cu(II)-IAPP complexes, EPR parameters for Cu(II)-IAPP complexes (tabulated data), the effect of Cu(II) in the amyloid aggregation of IAPP(15−22)H18A, comparison of EPR spectra for Cu(II)-fiber complexes and free Cu(II) in solution, and proposed Cu(II)-IAPP(15−22) equatorial coordination models (illustrated structures). This material is available free of charge via the Internet at http://pubs.acs.org.

AUTHOR INFORMATION

Corresponding Authors

*Phone: +52-55-57473723. E-mail: lilianaq@cinvestav.mx. (L.Q.)

*E-mail: lrivillas@uaem.mx. (L.R.-A.)

Notes

The authors declare no competing financial interest.

DOI: 10.1021/ic502945k
Inorg. Chem. 2015, 54, 3788−3796

■ ACKNOWLEDGMENTS

This research was funded by CONACYT (Grant Nos. 128255 and 221134). L.R.-A. and C.S.-L. thank CONACYT for postdoctoral and Ph.D. fellowships, respectively. The authors would also like to thank Sirenia González Posos (Microscopy Unit, LaNSE, Cinvestav), I.Q. Geiser Cuellar, for assistance with the acquisition of ESI-MS data, and LANEM facilities at CIQ-UAEM where the RMN data were collected.

■ REFERENCES

(1) Olefsky, J. M. *Endocrinology;* De Groot, L. J., Ed.; Saunders: London, U.K., 1989; Vol. 2, pp 1369−1399.
(2) Opie, E. L. *J. Exp. Med.* **1901**, *5*, 527−540.
(3) Westermark, G. T.; Wernstedt, C.; Wilander, E.; Sletten, K. *Biochem. Biophys. Res. Commun.* **1986**, *140*, 827−831.
(4) Westermark, P.; Wilander, E.; Westermark, G. T.; Jonhson, K. H. *Diabetologia* **1987**, *30*, 887−892.
(5) Lukinius, A.; Wilander, E.; Westermark, G. T.; Engstroem, U.; Westermark, P. *Diabetologia* **1989**, *32*, 240−244.
(6) Butler, P. C.; Chou, J.; Carter, W. B.; Wang, Y. N.; Chang, D.; Chang, J. K.; Rizza, R. A. *Diabetes* **1990**, *39*, 634−638.
(7) Hanabusa, T.; Kubo, K.; Oki, C.; Nakano, Y.; Okai, K.; Sanke, T.; Nanjo, K. *Diabetes Res. Clin. Pract.* **1992**, *15*, 89−96.
(8) Leckstrom, A.; Bjorklund, K.; Permert, J.; Larsson, R.; Westermark, P. *Biochem. Biophys. Res. Commun.* **1997**, *239*, 265−268.
(9) Enoki, S.; Mitsukawa, T.; Takemura, J.; Nakazato, M.; Aburaya, J.; Toshimori, H.; Matsukara, S. *Horm. Metab. Res.* **1992**, *15*, 97−102.
(10) Kautzky-Willer, A.; Tohomaseth, K.; Ludvik, B.; Nowotny, P.; Rabensteiner, D.; Waldhausl, W.; Pacini, G.; Prager, R. *Diabetes* **1997**, *46*, 607−614.
(11) Degano, P.; Silvestre, R. A.; Salas, M.; Peiro, E.; Marco, J. *Regul. Pept.* **1993**, *43*, 23−31.
(12) Chance, W. T.; Balasubramaniam, A.; Stallion, A.; Fischer, J. E. *Brain Res.* **1993**, *607*, 185−188.
(13) Harris, P. J.; Cooper, M. E.; Hiranyachattada, S.; Berka, J.; Jennifer, L.; Kelly, D. J.; Nobes, M.; Wookey, P. J. *Am. J. Pathol.* **1997**, *272*, F13−F21.
(14) Kahn, S. E.; Andrikopoulos, S.; Verchere, C. B. *Diabetes* **1999**, *48*, 241−253.
(15) Marzban, L.; Park, K.; Verchere, C. B. *Exp. Gerontol.* **2003**, *38*, 347−351.
(16) Betsholtz, C.; Christmansson, L.; Engstroem, U.; Frederik, S.; Viveka, J.; Kenneth, H.; Westermark, P. *FEBS Lett.* **1989**, *251*, 261−264.
(17) Westermark, P.; Engstroem, U.; Johnson, K. H.; Westermark, G. T.; Betsholtz, C. *Proc. Natl. Acad. Sci. U.S.A.* **1990**, *87*, 5036−5040.
(18) Jaikaran, E.; Clark, A. *Biochim. Biophys. Acta* **2001**, *1537*, 179−203.
(19) Nanga, R. P. R.; Brender, J. R.; Vivekanandan, S.; Ramamoorthy, A. *Biochim. Biophys. Acta* **2011**, *1808*, 2337−2342.
(20) Kayed, R.; Bernhagen, J.; Greenfield, N.; Sweimeh, K.; Brunner, H.; Voelter, W.; Kapurniotu, A. *J. Mol. Biol.* **1999**, *287*, 781−796.
(21) Yonemoto, I.; Kroon, G. J.; Dyson, H.; Balch, W. E.; Kelly, J. W. *Biochemistry* **2008**, *47*, 9900−9910.
(22) Goldsbury, C.; Goldie, K.; Pellaud, J.; Seelig, J.; Frey, P.; Muller, S.; Kistler, J.; Cooper, G.; Aebi, U. *J. Struct. Biol.* **2000**, *130*, 352−362.
(23) Jayasinghe, S. A.; Langen, R. *Biochemistry* **2005**, *44*, 12113−12119.
(24) Apostolidou, M.; Jayasinghe, S. A.; Langen, R. *J. Biol. Chem.* **2008**, *283*, 17205−17210.
(25) Wiltzius, J. J. W.; Sievers, S. A.; Sawaya, M. R.; Eisenberg, D. *Protein Sci.* **2009**, *18*, 1521−1530.
(26) DeToma, A. S.; Salamekh, S.; Ramamoorthy, A.; Hee Lim, M. *Chem. Soc. Rev.* **2012**, *41*, 608−621.
(27) Brender, J. R.; Hartman, K.; Nanga, R. P. R.; Popovych, N.; Bea, R. d. l. S.; Vivekanandan, S.; Marsh, E. N. G.; Ramamoorthy, A. *J. Am. Chem. Soc.* **2010**, *132*, 8973−8983.
(28) Hutton, J. C. *Diabetologia* **1989**, *32*, 271−281.
(29) Brender, J. R.; Krishnamoorthy, J.; Messina, G. M. L.; Deb, A.; Vivekanandan, S.; La Rosa, C.; Penner-Hahn, J. E.; Ramamoorthy, A. *Chem. Commun.* **2013**, *49*, 3339−3341.
(30) Salamekh, S.; Brender, J. R.; Hyung, S.-J.; Nanga, R. P. R.; Vivekanandan, S.; Brandon T. Ruotolo, B. T.; Ramamoorthy, A. *J. Mol. Biol.* **2011**, *410*, 294−306.
(31) Zargar, A. H.; Shah, N. A.; Masoodi, S. R.; Laway, B. A.; Dar, F. A.; Khan, A. R.; Sofi, F. A.; Wani, A. I. *Postgrad. Med. J.* **1998**, *74*, 665−668.
(32) Rodríguez Flores, C.; Preciado Puga, M.; Wrobel, K.; Garay Sevilla, M. E.; Wrobel, K. *Diabetes Res. Clin. Pract.* **2011**, *91*, 333−341.
(33) Tanaka, A.; Kaneto, H.; Miyatsuka, K.; Yamamoto, K.; Yoshiuchi, K.; Yamasaki, Y.; Shimomura, I.; Matsuoka, T.; Matsuhisa, M. *Endocr. J.* **2009**, *56*, 699−706.
(34) Naka, T.; Kaneto, H.; Katakami, N.; Matsuoka, T.; Harada, A.; Yamasaki, Y.; Matsuhisa, M.; Shimomura, I. *Endocr. J.* **2013**, *60*, 393−396.
(35) Kazi, T. G.; Afridi, H. I.; Kazi, N.; Jamali, M. K.; Arain, M. B.; Jalbani, N.; Kandhro, G. A. *Biol. Trace Elem. Res.* **2008**, *122*, 1−18.
(36) Janciauskiene, S.; Ahren, B. *Biochem. Biophys. Res. Commun.* **2000**, *267*, 619−625.
(37) Ma, L.; Li, X.; Wang, Y.; Zheng, W.; Chen, T. *J. Inorg. Biochem.* **2014**, *140*, 143−152.
(38) Masad, A.; Hayes, L.; Tabner, B. J.; Turnbull, S.; Cooper, L. J.; Fullwood, N. J.; German, M. J.; Kametani, F.; El-Agnaf, O. M.; Allsop, D. *FEBS Lett.* **2007**, *581*, 3489−3493.
(39) Yu, Y.-P.; Lei, P.; Hu, J.; Wu, W.-H.; Zhao, Y.-F.; Li, Y.-M. *Chem. Commun.* **2010**, *46*, 6909−6911.
(40) Lee, E. C.; Ha, E.; Singh, S.; Legesse, L.; Ahmad, S.; Karnaukhova, E.; Donaldsona, R. P.; Jeremic, A. M. *Phys. Chem. Chem. Phys.* **2013**, *15*, 12558−12571.
(41) Bellia, F.; Grasso, G. *J. Mass Spectrom.* **2014**, *49*, 274−279.
(42) Exley, C.; Mold, M.; Shardlow, E.; Shuker, B.; Ikpe, B.; Wu, L.; Fraser, P. E. *J. Diabetes Res. Clin. Metab.* **2012**, *1*, 1−6.
(43) Mirhashemi, S. M.; Shahabaddin, M.-E. *Pak. J. Biol. Sci.* **2011**, *14*, 288−292.
(44) Ward, B.; Walker, K.; Exley, C. *J. Inorg. Biochem.* **2008**, *102*, 371−375.
(45) Sinopoli, A.; Magri, A.; Milardi, D.; Pappalardo, M.; Pucci, P.; Flagiello, A.; Titman, J. J.; Nicoletti, V. G.; Caruso, G.; Pappalardo, G.; Grasso, G. *Metallomics* **2014**, *6*, 1841−1852.
(46) Sigel, H.; Martin, R. B. *Chem. Rev.* **1982**, *82*, 385−426.
(47) Kállay, C.; Dávid, A.; Timári, S.; Nagy, E. M.; Sanna, D.; Garribba, E.; Micera, G.; De Bona, P.; Pappalardo, G.; Rizzarelli, E.; Sóvágó, I. *J. Chem. Soc., Dalton Trans.* **2011**, *40*, 9711−9721.
(48) Rivillas-Acevedo, L.; Grande-Aztatzi, R.; Lomelí, I.; García, J. E.; Barrios, E.; Teloxa, S.; Vela, A.; Quintanar, L. *Inorg. Chem.* **2011**, *50*, 1956−1972.
(49) Daniele, P. G.; Prenesti, E.; Ostacoli, G. *J. Chem. Soc., Dalton Trans.* **1996**, 3269−3275.
(50) Peisach, J.; Blumberg, W. E. *Arch. Biochem. Biophys.* **1974**, *165*, 691−708.
(51) Alexandrescu, A. T. *PLoS One* **2013**, *8*, 1−8.
(52) Clore, G. M.; Iwahara, J. *Chem. Rev.* **2009**, *109*, 4108−4139.
(53) Quintanar, L.; Rivillas-Acevedo, L.; Grande-Aztatzi, R.; Gomez-Castro, C. Z.; Arcos-Lopez, T.; Vela, A. *Coord. Chem. Rev.* **2013**, *257*, 429−444.
(54) Bedrood, S.; Li, Y.; Isas, J. M.; Hegde, B. G.; Baxa, U.; Haworth, I. S.; Langen, R. *J. Biol. Chem.* **2012**, *287*, 5235−5241.
(55) Wiltzius, J. J. W.; Sievers, S. A.; Sawaya, M. R.; Cascio, D.; Popov, D.; Riekel, C.; Eisenberg, D. *Protein Sci.* **2008**, *17*, 1467−1474.
(56) Cao, P.; Abedini, A.; Raleigh, D. P. *Curr. Opin. Struct. Biol.* **2013**, *23*, 82−89.
(57) He, L.; Wang, X.; Zhao, C.; Wang, H.; Du, W. *Metallomics* **2013**, *5*, 1599−1603.
(58) Kemtemourian, L.; Domenech, E.; Doux, J. P. F.; Koorengevel, M. C.; Killian, J. A. *J. Am. Chem. Soc.* **2011**, *133*, 15598−15604.

DOI: 10.1021/ic502945k
Inorg. Chem. 2015, 54, 3788−3796